A MUTI-PHASE SPH-HBP-DP METHOD FOR SIMULATING THE PROGRESSIVE ENTRAINMENT BEHAVIOR OF DEBRIS FLOW CONSIDERING THE DYNAMIC ATTENUATION OF SOIL STRENGTH

YANGFAN MA[1], MITSUTERU ASAI[1], ZHENG HAN[2] AND GUANGQI CHEN[13]

[1] Graduate School of Civil Engineering, Kyushu University,
744 Motooka Nishi-ku, Fukuoka
819-0395, Fukuoka, Japan
e-mail: asai@doc.kyushu-u.ac.jp

[2] School of Civil Engineering, Central South University,
22 Shaoshan South Road, Tianxin District, Changsha
410075, Hunan, China
e-mail: zheng_han@csu.edu.cn

[3] School of Civil and Transportation Engineering, Hebei University of Technology
5340 Xiping Road, Beichen District, Tianjin
300000, Tianjin, China
email: chen@artsci.kyushu-u.ac.jp

Abstract. Debris flows overriding steep valleys can cause a significant decrease in bed friction resistance due to undrained excess pore water pressure, leading to an exponential increase in both destructiveness and volume. This study develops a two-phase numerical model based on Smoothed Particle Hydrodynamics to simulate the progressive entrainment behavior of debris flow accurately. The fluid and bed-sediment materials are modeled using the non-Newtonian Bingham-type Herschel-Bulkley-Papanastasiou (HBP) constitutive model. The mass erosion behavior of debris flow is achieved and augmented by incorporating the Drucker-Prager (DP) softening model, which accounts for variations in the pore water pressure ratio across different saturation states. A straightforward phase-change approach is implemented according to the mutation of effective viscosity to prevent any minute displacements of viscoplastic materials when subjected to steep inclinations. The multi-phase model has been compared with the large-scale flume experiments conducted by the United States Geological Survey. The 3-D numerical results obtained from the rigid bed, dry and wet erodible bed exhibit a good agreement with the experimental data, encompassing flow momentum feedback and erosion patterns. This paper initially attempts to simulate the entrainment of multiple phases in a steep valley by incorporating viscoplastic flow.

Keywords: Debris Flow, Progressive Entrainment, SPH, Drucker-Prager Criterion, Shear Strengthen Reduction, Phase Change

1 INTRODUCTION

Analyses of erosion, entrainment, and deposition process between gravity-driven mixture flows and the underlying sediment layer assist in interpreting the dynamics of earth flow, deposition morphology, and landscape formation [1,2]. The occurrence of intricate processes, such as landslides, debris flows, and process chains, poses a significant threat to human settlements and infrastructure on a global scale [3]. Triggered by geological events (e.g., earthquake, landslides) or hydraulic replenishment, the destructive potential of debris flows is directly proportional to the volume of mass transferred, and entrained material can accumulate multiple times its original volume along the trajectory [4,5]. Regarding this phenomenon, the predominant explanation currently among researchers is that the saturated state of sediment deposition, specifically the undrained excess pore water pressure, significantly influences soil mechanism, as supported by several studies [5-7]. This influence, in turn, controls the exchange of mass and momentum between the overlying debris flow and the bed sediment. Nonetheless, a systematic comprehension of the development of pore pressure response and the mechanism of soil strength mutation during progressive entrainment remains deficient. This is primarily attributed to debris flows' diverse composition (i.e., water, sand, and boulders) and complex nature (i.e., Newtonian fluids, non-Newtonian fluids, and solids).

Erosion patterns, including floc erosion, surface erosion, and mass erosion (entrainment), are commonly differentiated based on the relative contributions of turbulent flow hydrodynamics and dynamic pressure to bed failure [8]. In hyper-concentrated flows with high velocity, frequent interparticle contact dominates the friction behaviour of debris flow, referred to as the grain-inertia regime [9], where mass erosion will serve as the primary erosion mode. In contrast, the viscosity of the interstitial fluid has a negligible effect [10]. This conclusion can be further supported and the differences between the two modes can be highlighted by comparing their respective erodible dam-break tests: the Louvain experiment [11] and the granular step collapse [12].

A series of large-scale flume tests, carried out by the United States Geological Survey (USGS) [5,13], have produced remarkable outcomes indicating that increased flow momentum and speed only occur with positive feedback when the bed sediments are sufficiently wet. The relatively drier sediment, in contrast, result in negative feedback and decrease the flow momentum. Another experimental study [14] has drawn a similar conclusion, highlighting the impact force enhancement. Recent researches have begun to deduce the pattern of soil strength reduction by establishing correlations with factors such as velocity [15], deviatoric plastic strain [16], and distortional strain [17].

Previous numerical research on the subject has been mostly restricted to shallow water equations (SWEs) assumption, commonly known as the “depth-averaged approach”. The approach entails homogenizing the velocity profile along the depth direction, reducing dimensions and increasing cost-effectiveness. One alternative approach is integrating a three-dimensional, particle-based numerical model with appropriate yielding criterion, which captures basal shear and ploughing effect. Erosion is currently evaluated based on the field variable carried by each particle, rather than the erosion rate. Several exemplary methods have been employed to study pure water erosion within the Smoothed Particle Hydrodynamics (SPH) framework [18-20].

In the literature, many rheological models are commonly employed to simulate dense granular fluids. Typical examples include elastic–plastic model [21,22] and elastic–viscoplastic model [20]. These methods face challenges in accurately capturing the intermediate state of the fluid-solid transition, partly due to the complexities involved in handling stress scaling and tension cracking. Given the dependence of granular materials on yield criteria and shear rate, they exhibit closer similarities to classical viscoplastic fluids. Remarkable examples include the series models of non-Newtonian Bingham-type family [18,23,24], and $\mu(I)$ rheological model [25]. These types of models typically represent the viscosity stress tensor as a function of effective (apparent) viscosity and strain rate tensor. It is worth noting that these models do not require an additional explicit elastic branch to capture the intermediate dense regime [18]. The Mohr-Coulomb (MC) criterion is widely used in the geotechnical engineering and combined with the rheological model in viscoplastic materials. However, researchers lean towards using the Drucker-Prager (DP) criterion in particle methods as a smooth alternative. Another critical study [26] reveals that the MC criterion was more conservative in particle movement.

In this study, both the overlying fluid and bed are modeled as a non-Newtonian Bingham viscoplastic material employing the HBP constitutive model. The Drucker-Prager yield criterion is chosen to model bed-sediment because it can accurately capture yield surface. The Mohr-Coulomb criterion is incorporated with HBP to simulate debris flow. This study presents the initial attempt to simulate multi-phase entrainment in a steep valley involving viscoplastic flow. Shear strength reduction is evaluated by directly approximating the pore water pressure ratio [27], which is then incorporated into a Drucker-Prager softening model to model the mass erosion behavior. Additionally, a straightforward phase-change approach is implemented based on the mutation of effective viscosity to prevent any minute displacements of viscoplastic materials in steep valleys.

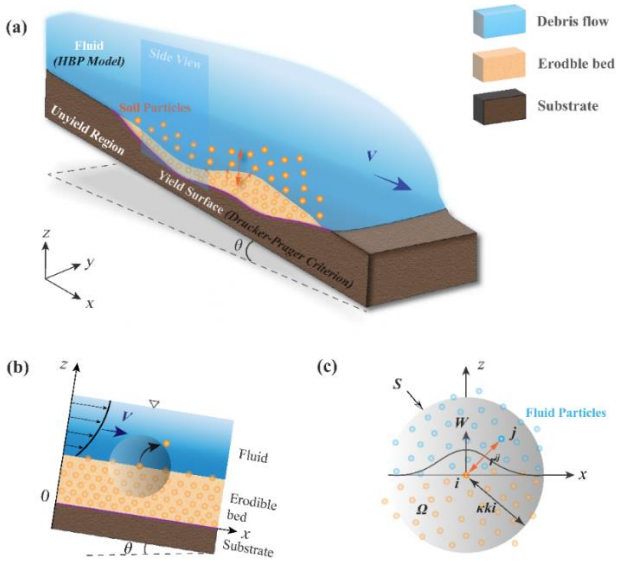

Fig. 1: Schematic of (a) two-phase debris flow SPH model and (b) side view of the particle interaction and (c) discretization of the two-phase particles within support domain.

2 NUMERICAL MODEL

The physical simulation domain closely resembles the two-layer model proposed by Iverson et al [1]. as depicted in **Fig. 1**. The bottom layer consists of a completely static and immovable geological substrate. In the model, it is composed of boundary particles and completely yielding soil particles. The erodible layer between the yielding surface and the soil-water interface is governed by the non-Newtonian rheological model and the Drucker-Prager yield criterion. It demonstrates a gradual decrease in velocity with increasing depth influenced by the pressure-dependent yielding criterion. The overlying fluid portion and the sediment soil particles share the same rheological model. The yield stress, conversely, is determined by the Mohr-Coulomb yield criterion derived from our previous studies [28,29] of the HBP-SPH model. This portion consists of fluid particles with some entrained soil particles. The following sections describe how these regions are treated using SPH.

2.1 Governing equations and SPH discretization

The SPH method is employed as the spatial discretization technique for all equations in this study. Detailed derivations of the SPH approximations can be found in previous research [18,19]. This study starts with the Governing equations. The continuity and momentum equations are described by the Lagrangian form of the Navier-Stokes equations, which are discretized using the SPH scheme. Greek superscripts α, β denote coordinate directions through the utilization of Einstein's summation:

$$\frac{d\rho_i}{dt} = \rho_i \sum_{j=1}^{N} \frac{m_j}{\rho_j} \left(u_i^\alpha - u_j^\alpha\right) \frac{\partial W_{ij}}{\partial x^\alpha}, \tag{1.1}$$

$$\frac{du_i^\alpha}{dt} = -\sum_{j=1}^{N} m_j \left(\frac{P_i + P_j}{\rho_i \rho_j}\right) \frac{\partial W_{ij}}{\partial x_i^\alpha} + \sum_{j=1}^{N} m_j \left(\frac{\tau_i^{\alpha\beta} + \tau_i^{\alpha\beta}}{\rho_i \rho_j}\right) \frac{\partial W_{ij}}{\partial x_i^\beta} + g^\alpha \tag{1.2}$$

where ρ denotes the phase density and u is the velocity, g refers to the gravitational force. subscript i and j refers to the interpolating and neighboring particles respectively, m_j is the mass and W_{ij} signifies the quantic Wendland kernel. The viscosity stress tensor $\tau_i^{\alpha\beta}$ is obtained according to the rheological model considering different phases. σ is the total stress tensor which is constitutive of the isotropic pressure p and viscous stress τ, can be written as:

$$\sigma^{\alpha\beta} = p\delta^{\alpha\beta} + \tau^{\alpha\beta}, \tag{1.3}$$

with $\delta = 1$ for $\alpha = \beta$ and 0 otherwise, δ represent the Kronecker's delta function.

In the WCSPH scheme, the Tait's equation of state is employed to link pressure to the density through the following equation:

$$p = \frac{C_{s0}^2 \rho_0}{\gamma} \left[\left(\frac{\rho}{\rho_0}\right)^\gamma - 1\right], \tag{1.4}$$

with ρ_0 the reference density of the phase, C_{s0} the numerical speed of the sound and γ the polytropic index set to 7 in this study.

2.2 Weakly-compressible scheme

2.2.1 Boundary treatment

Typical viscoplastic fluid exhibit no-slip behavior on the basal rigid boundaries. However, Both the in-situ survey and experiments demonstrate that during the downhill movement of granular materials, even the bottommost layer of particles in contact with the bottom boundary exhibits non-zero velocity. Despite many partial-slip boundary method [30] proposed in recent year, complex treatment of boundary projection is still necessary. This complexity increases computational load and relies on subjective judgments regarding the degree of slip. This study employs the Dynamic boundary conditions (DBC) [31] and approximate the no-slip condition by setting the boundary velocity to zero. The DBC offers straightforward computational implementation and compatibility with arbitrarily complex geometries.

2.2.2 Time integration

The explicit second-order Verlet scheme is used for the time integration in the proposed numerical model, and the CFL condition bounds the variable time step algorithm with an extra restriction imposed by viscous forces, which can be written as:

$$\Delta t = Co \min\left(\min_i \sqrt{\frac{h}{|f_i|}}, \frac{h}{C_{s0}}, \frac{h^2}{v} \right), \tag{2.5}$$

with Co the Courant number and f_i the force increment of particle i, v refers to the kinematic viscosity. Both phases employ the same time integration scheme, with the minimum time step determined by the CFL condition.

3 TWO PHASE MODELLING OF THE DEBRIS FLOW

3.1 Constitutive model and yield criterion

The Herschel-Bulkley-Papanastasiou (HBP) model [32] is employed to model the rheological characteristics of both overriding fluid and bed sediment. We initially revisit Eq. (2.3) for the viscosity term as Newtonian constitutive equation:

$$\tau_i^{\alpha\beta} = 2\mu_{HBP}\varepsilon_i^{\alpha\beta}, \tag{3.1}$$

where $\dot{\varepsilon}_i^{\alpha\beta}$ denotes the strain rate tensor and μ_{HBP} the effective viscosity. In the WCSPH scheme they can be expressed as:

$$\mu_{HBP} = \frac{|\tau_y|}{\sqrt{\prod_D}}\left[1 - e^{-m\sqrt{\prod_D}}\right] + 2\mu\left|4\prod_D\right|^{\frac{n-1}{2}}, \tag{3.2}$$

$$\dot{\varepsilon}^{\alpha\beta} = \frac{1}{2}\left[\frac{\partial u^\alpha}{\partial x^\beta} + \frac{\partial u^\beta}{\partial x^\alpha}\right] - \frac{1}{3}\left[\frac{\partial u^\gamma}{\partial x^\gamma}\right]\delta^{\alpha\beta}, \tag{3.3}$$

where τ_y denotes the yield stress and $\prod_D$ the second invariant of the strain rate tensor, and $\delta^{\alpha\beta}$ the Kronecker's delta function. m governs the exponential growth of stress and n is the power law index facilitating the simulation of dilatant and pseudoplastic fluids.

The HBP constitutive model, integrated with the MC criterion, is a preferred choice for

modeling the dynamic behavior of debris flow due to its capability in accurately simulate runout extent and flow thickness [29]. However, previous research [26] has shown that the Mohr-Coulomb criterion tends to be conservative and exhibits discontinuities in determining the yield of bed sediment. Another pressure-dependent model, the DP criterion is chosen as a smooth alternative for sediment soil particles, which can be mathematically represented as:

$$\tau_y = -\alpha p + \kappa, \tag{3.4}$$

$$\alpha = -\frac{2\sqrt{3}\sin(\varphi)}{3-\sin(\varphi)},\ \kappa = \frac{2\sqrt{3}c\cos(\varphi)}{3-\sin(\varphi)}. \tag{3.5}$$

This methodology treats the non-yield sediment particles at subsurface layers as a fix boundary. Our investigation has revealed that while this particular substance exhibits satisfactory performance on even terrain, it cannot mitigate the minute displacement of viscoplastic fluids when subjected to steep inclinations using the DP criterion. In this study, we propose a straightforward method to address soil particle collapse by utilizing the identified mutation of effective viscosity in the initial exponential stage of the HBP constitutive model. It is imperative to re-examine Eq. (3.2) first term of the right hand satisfies:

$$\lim_{\varepsilon\to 0}\frac{|\tau_y|}{\sqrt{\Pi_D}}\left[1-e^{-m\sqrt{\Pi_D}}\right] = m|\tau_y|. \tag{3.6}$$

During the initial stage, as the strain rate approaches zero, the contribution of the Papanastasiou term (the second term of the right hand of Eq. (3.2)) becomes negligible. At the same time, the effective viscosity is predominantly determined by the Herschel-Bulkley term. At this stage,
It is obvious that the material is currently in the non-yielding phase of viscoplastic behavior, and the effective viscosity is exceptionally elevated. However, once the transition to a stage with a significantly high strain rate occurs, the importance of the Papanastasiou term becomes impossible to overlook and signaling the onset of yielding.

3.2 Shear strength reduction pattern

Terzaghi's principle indicates that in a drained condition, the total pressure p_{tot} acting on saturated soil is composed of pore water pressure p_{pw} and effective (skeleton) pressure p_{eff}. Hence, Eq. (3.4) is revisited:

$$\tau_y = -\alpha\left(p_{tot} - p_{pw}\right) + \kappa, \tag{3.7}$$

Typically, the measurement of pore water pressure requires the prior detection of the soil-water interface and free surface to determine the hydraulic head pressure difference. A study conducted by Manenti et al [33] demonstrates that the computation involved in such an attempt is costly and leads to inaccurate results due to the significant deformation of the interface. A low-cost approach [18] is utilized by establishing a connection between the pore water pressure and the pressure exerted by the saturated sediment:

$$p_{i,pw} = \frac{C_{s0,w}^2\rho_{0,w}}{\gamma_w}\left[\left(\frac{\rho_{i,sat}}{\rho_{0,sat}}\right)^{\gamma} - 1\right], \tag{3.8}$$

where *w* and *sat* refers to the water and saturated sediment phase respectively. Finally, the skeleton pressure can be determined by calculating the total and pore water pressures using Eq. (1.4) and (3.8). Our objective is to establish a correlation between pore pressure and the DP criterion in order to examine the reduction in shear resistance within an erodible bed caused by the development of excess pore pressures. The section regarding the internal friction angle in Eq. (3.5) will be examined here:

$$\tan\varphi = (1-\lambda)\tan\varphi', \tag{3.9}$$

where $\lambda = p_{pw}/p_{tot}$ refers to the pore pressure ratio [27] and φ' is the effective friction angle. Eq. (3.9) suggests that the effective friction angle inherently captures the influence of pore pressures. The Mohr-Coulomb softening model inspires this reported in Hervé et al [17]. When sediment soil particles are yielding, with at least one fluid particle within their support domain, the effective internal friction angle of shear stress will be updated based on Eq. (3.5) and (3.9). Consequently, the parameter λ increases with the rise in pore water pressure, leading to a decrease in the bed-sediment shear resistance.

4 CASE STUDY

4.1 Overview of the USGS flume experiment

The large-scale flume experiment of Iverson et al. [5,13] represents the entrainment process of debris flow under different configurations. A total of 163 experiments were conducted by the United States Geological Survey (USGS) from 1992 to 2017. This study investigated three groups: debris flow on a rigid bed, debris flow on an erodible dry bed, and debris flow on an erodible saturated bed as comparative research subject.

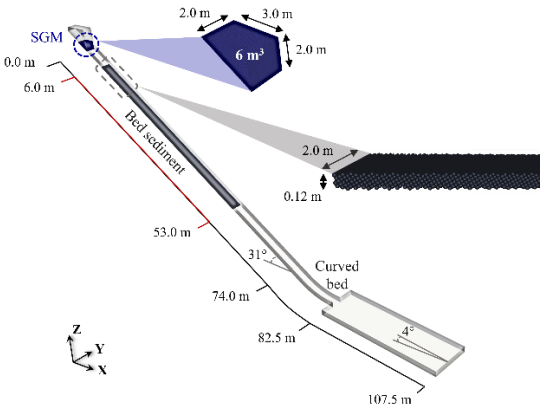

Fig. 2 A sketch of the geometric model for USGS flume experiment.

As shown in **Fig. 2**, a rectangular concrete channel with a size of 95 m long, 2 m wide, and 1.2 m depth is inclined at an angle of 31° from the horizontal. Longitudinal distances in the flume (x) are referenced relative to the front position of the released debris column located at $x = 15$ m. A vertical top gate is positioned at the upper part of the flume channel with a height of 2 meters, to retain static debris before release. The flume bed begins to flatten from the

position at $x = 74$ m, gradually decreasing to $4°$ after reaching the flume mouth at $x = 82.5$ m. The flume bottle is almost entirely covered with bumpy concrete tiles to increase the roughness of the surface. The water-saturated debris-flow mass with a volume of 6 m^3 is discharged abruptly from a headgate. As required, cover a section of partially saturated sediment in the middle of the flume with a length of 47 m and an average depth of 12 cm. The debris flow and the bed sediment consist of a mixture composed of gravel, sand, and mud-sized grains referred to as SGM. More details pertaining to the setup of the flume experiment and the composition of materials can refer to previous studies [13].

4.2 Simulation results

The proposed Multi-phase SPH-HBP-DP method is employed to simulate the large-scale USGS flume experiment. The flume is regarded as a boundary comprised of fixed particles, while the debris flow and bed sediment are discretized into multiple non-Newtonian type particles. Our study revealed that the initial particle distance influences the obtained outcomes. However, the sensitivity analysis of the parameters is beyond the scope of the current paper's discussion. This study set the initial particle spacing as 0.03 m, with a total of 1,012,083 boundary particles, 206,250 debris-flow particles, and 439,987 sediment particles generated. Other parameters regarding materials information and simulation configuration are summarized in **Table 1**.

We compared the experimental and numerical results of three different configurations, corresponding to the scenarios of debris flow on a rigid bed, an erodible dry bed, and a saturated erodible bed. **Fig. 3** illustrates the results of the time-elapsed simulation depicting the dynamic behavior of the debris-flow mass on a rigid bed. The figure demonstrates that following the opening of the flume headgate, similar to a dam-break, the rapid collapse and advancement cause a rapid acceleration, resulting in an elongated and thinner front of the debris flow. This state exhibits thinner and more diluted characteristics. Following the initial 5 seconds, this characteristic further leads to local fluid discontinuity. At approximately the 10-second mark, the foremost part of the debris flow enters the curvature transition zone inside the flume, initiating a process of deceleration. Upon exiting the flume outlet and entering the nearly planar concrete surface, its velocity gradually diminishes, leading to limited sediment deposition.

Table 1 Summary of the debris and bed material parameters

Materials parameters		Notation	Unit	Value
Debris flow	Density	ρ_f	Kg/m^3	1650
	Kinematic viscosity	υ	m^2/s	0.02
	Exponential index	m	/	100
	Power law index	n	/	1
	Cohesion	c_f	Pa	0
	Internal friction angle	φ_f	°	40
Bed sediment	Density	ρ_b	Kg/m^3	1650
	Saturated density	ρ_{sat}	Kg/m^3	1750
	Kinematic viscosity	υ	m^2/s	0.02
	Exponential index	m	/	100
	Power law index	n	/	1
	Cohesion	c_f	Pa	1
	Internal friction angle	φ_f	°	40

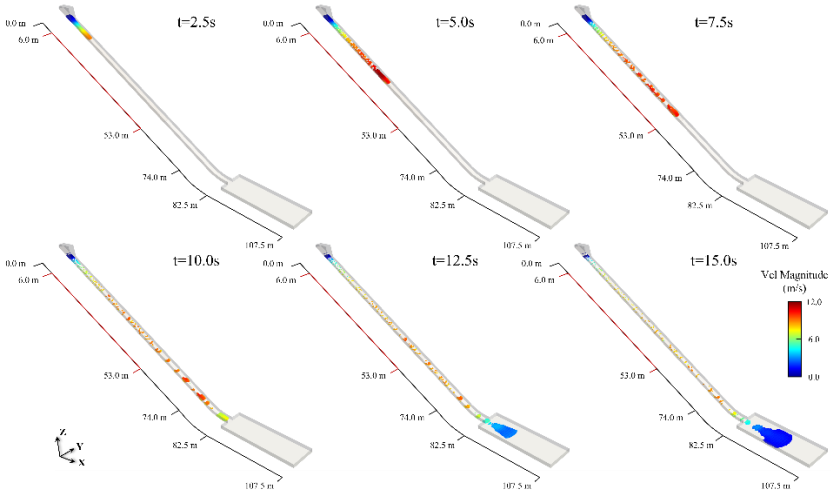

Fig. 3 Snapshots of the USGS experiment of debris-flow motion on rigid bed.

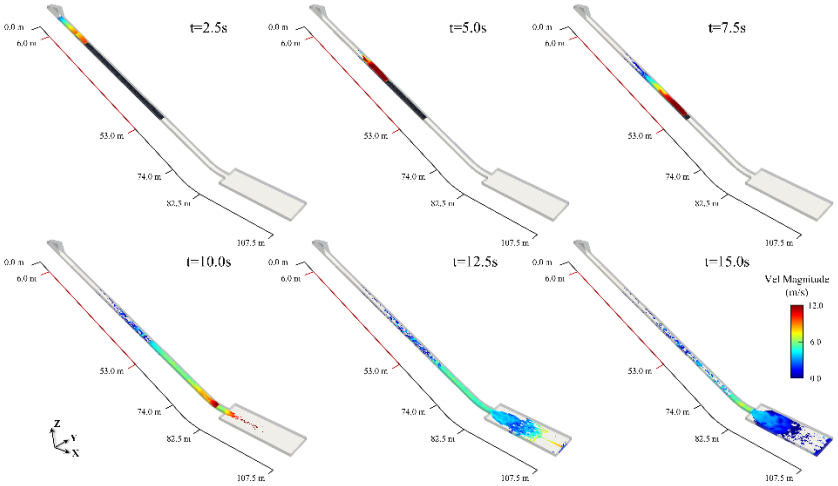

Fig. 4 Snapshots of the USGS experiment of debris-flow motion on wet erodible bed.

Fig. 4 and **Fig. 5** respectively demonstrate the dynamic processes of debris flow in wet and dry erodible bed-sediment scenarios. Based on the effective stress mutation treatment of the HBP model, the bed sediment can be fully stabilized on the steeply inclined channel with minimal slip. Shear strength reduction is implemented in the wet erodible scenario once the overriding flow contacts the bed sediment. As depicted in **Fig. 4**, the effects of bed sediment on flow behavior became conspicuous. In the early stages of encountering bedload sediment, there is a slight decrease in the velocity of the mixed material (t=2.5s). However, as the pore water pressure within the non-drained bed sediment increases, it reduces shear resistance, which eventually leads to self-propelled entrainment and an increase in momentum. Over time, the velocity of the mixed materials continues to increase, surpassing the front position of the control group with a rigid bed surface before exiting the flume outlet (t=10.0s). Ultimately, the flow entrained almost all the bed sediment in the upstream, with only a small amount of residue

remaining on both sides of the channel. Compared to the rigid bed group, a significantly larger run-out extent was observed under the condition of a saturated erodible bed (t=15.0s).

The situation is completely reversed in the dry bed scenario. The strength of the bed sediments, precisely the angle of internal friction, remains constant. As depicted in **Fig. 5**, upon encountering a dry bed material, the debris flow velocity progressively decreases from a maximum of 8 m/s to approximately 3 m/s. It is evident that until the 15-second mark, the front portion of the debris flow has not yet exited the channel outlet. Evident mass erosion was observed solely in the upstream section spanning 6-15m, with considerable residual sediment present along both channel banks.

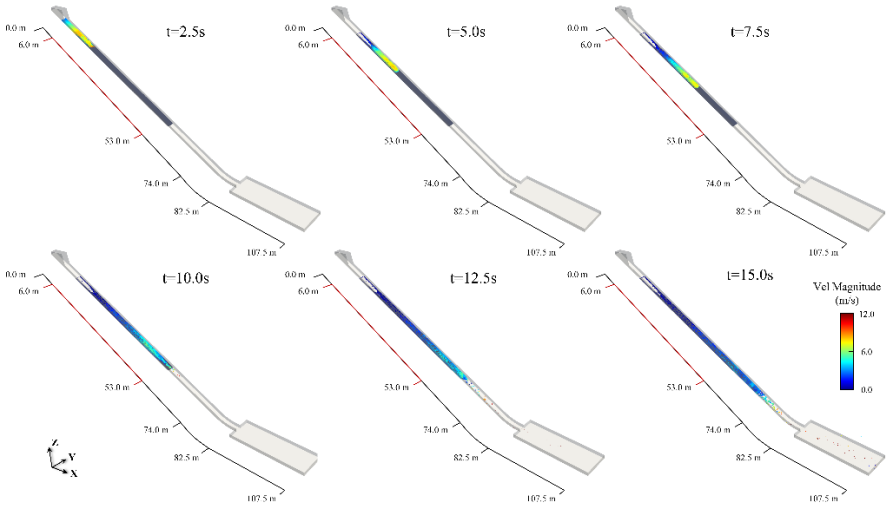

Fig. 5 Snapshots of the USGS experiment of debris-flow motion on dry erodible bed.

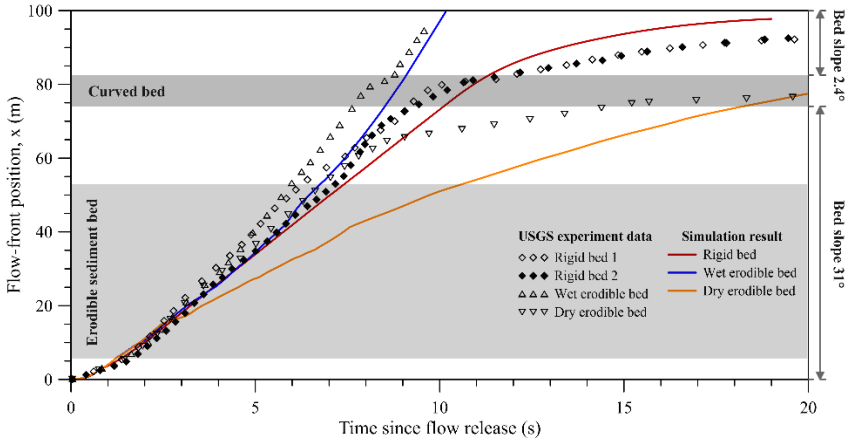

Fig. 6 Debris-flow front position propagation, compared with the experimental data[5].

Fig. 6 presents the debris-flow front position propagation between simulation and experiment data. It can be inferred that, during the initial release of the debris flow, the flow velocity and spatial position development of the three control groups exhibited a high level of consistency before encountering the bed sediment. The manifestation of the debris flow

behavior's response to sediment configuration becomes evident from 3s, and the flows that encounter the wet erodible bed (blue line) exhibit an almost explosive behavior, with a continuous increase in velocity. Once the bottom friction resistance and acceleration have reached equilibrium, the velocity of the rigid bed group (red line) transitions into a stable phase until reaching the curved bed section, where the flow velocity experiences a notable decrease and gradually accumulates after exiting the flume outlet. In contrast, flows that encounter the dry erodible bed (yellow line) experience a significant decrease in flow velocity upon entering the erosion area.

5 CONCLUSIONS

This paper proposes a three-dimensional SPH-HBP-DP method to model the progressive entrainment behavior of debris flow. Two crucial issues are addressed: stabilizing viscoplastic materials on slopes and achieving a seamless solid-fluid transition. Additionally, the study focuses on simulating the strength attenuation during the non-drainage loading process, facilitating dynamic erosion simulation of debris flows in realistic scenarios.

The overriding mass and bed-sediment are modeled by the non-Newtonian type of Herschel-Bulkley-Papanastasiou constitutive model but facilitated with different yield criteria. The Drucker-Prager yield criterion is integrated into the rheological model. The shear resistance reduction is achieved by introducing the pore water pressure ratio into the internal friction angle, thereby transforming the DP model into a softening model. Compared to the commonly used numerical approach for soil sediment, the proposed method can define yield regions without the need for an additional explicit elastic branch. The proposed method is validated through a selected case study of a large-scale flume experiment conducted by the United States Geological Survey. The simulation results significantly agree with the experimental data for rigid, wet, and dry erodible beds.

REFERENCES

[1] Iverson, R.M. Elementary theory of bed-sediment entrainment by debris flows and avalanches. *J. Geophys. Res-Earth* (2012) **117**.

[2] Pudasaini, S.P. and Fischer, J.T. A mechanical erosion model for two-phase mass flows. *Int. J. Multiphas. Flow* (2020) **132**: 103416.

[3] Han, Z., Chen, G., Li, Y. *et al.* Numerical simulation of debris-flow behavior incorporating a dynamic method for estimating the entrainment. *Eng. Geol* (2015) **190**: 52-64.

[4] Iverson, R.M. and Ouyang, C. Entrainment of bed material by Earth‐surface mass flows: Review and reformulation of depth‐integrated theory. *Rev. Geophys* (2015) **53**: 27-58.

[5] Iverson, R.M., Reid, M.E., Logan, M. *et al.* Positive feedback and momentum growth during debris-flow entrainment of wet bed sediment. *Nat. Geosci* (2011) **4**: 116-121.

[6] Tayyebi, S.M., Pastor, M. and Stickle, M.M. Two-phase SPH numerical study of pore-water pressure effect on debris flows mobility: Yu Tung debris flow. *Comput. Geotech* (2021) **132**: 103973.

[7] Zheng, H., Shi, Z., Hanley, K.J. *et al.* Pore pressure evolution in bed sediment overridden by debris flow: A general formulation. *Earth Surf. Proc. Land* (2023) **48**: 1188-1201.

[8] Winterwerp, J., Van Kesteren, W., Van Prooijen, B. *et al.* A conceptual framework for shear flow–induced erosion of soft cohesive sediment beds. *J. Geophys. Res-Oceans* (2012) **117**.

[9] Bagnold, R.A. Experiments on a gravity-free dispersion of large solid spheres in a Newtonian fluid under shear in *Proceedings of the Royal Society of London. Series A. Mathematical and Physical Sciences.* **225**(1160): 49-63.

[10]Armanini, A., Fraccarollo, L. and Rosatti, G. Two-dimensional simulation of debris flows in erodible channels. *Comput. Geosci-UK* (2009) **35**: 993-1006.
[11]Fraccarollo, L. and Capart, H. Riemann wave description of erosional dam-break flows. *J. Fluid Mech* (2002) **461**: 183-228.
[12]Crosta, G., Imposimato, S. and Roddeman, D. Numerical modeling of 2‐D granular step collapse on erodible and nonerodible surface. *J. Geophys. Res-Earth* (2009) **114**.
[13]Iverson, R.M., Logan, M., LaHusen, R.G. *et al.* The perfect debris flow? Aggregated results from 28 large‐scale experiments. *J. Geophys. Res-Earth* (2010) **115**.
[14]Vicari, H., Ng, C.W., Nordal, S. *et al.* The effects of upstream flexible barrier on the debris flow entrainment and impact dynamics on a terminal barrier. *Can. Geotech. J* (2022) **59**: 1007-1019.
[15]Lee, K. and Jeong, S. Large deformation FE analysis of a debris flow with entrainment of the soil layer. *Comput. Geotech* (2018) **96**: 258-268.
[16]Lee, K., Kim, Y., Ko, J. *et al.* A study on the debris flow-induced impact force on check dam with-and without-entrainment. *Comput. Geotech* (2019) **113**: 103104.
[17]Vicari, H., Tran, Q.A., Nordal, S. *et al.* MPM modelling of debris flow entrainment and interaction with an upstream flexible barrier. *Landslides* (2022) **19**: 2101-2115.
[18]Fourtakas, G. and Rogers, B. Modelling multi-phase liquid-sediment scour and resuspension induced by rapid flows using Smoothed Particle Hydrodynamics (SPH) accelerated with a Graphics Processing Unit (GPU). *Adv. Water, Resour* (2016) **92**: 186-199.
[19]Zubeldia, E.H., Fourtakas, G., Rogers, B.D. *et al.* Multi-phase SPH model for simulation of erosion and scouring by means of the shields and Drucker–Prager criteria. *Adv. Water, Resour* (2018) **117**: 98-114.
[20]Ghaïtanellis, A., Violeau, D., Ferrand, M. *et al.* A SPH elastic-viscoplastic model for granular flows and bed-load transport. *Adv. Water, Resour* (2018) **111**: 156-173.
[21]Bui, H.H., Sako, K. and Fukagawa, R. Numerical simulation of soil–water interaction using smoothed particle hydrodynamics (SPH) method. *J. Terramechanics* (2007) **44**: 339-346.
[22]Manenti, S., Amicarelli, A. and Todeschini, S. WCSPH with limiting viscosity for modeling landslide hazard at the slopes of artificial reservoir. *Water* (2018) **10**: 515.
[23]Nikooei, M. and Manzari, M.T. Studying effect of entrainment on dynamics of debris flows using numerical simulation. *Comput. Geosci-UK* (2020) **134**: 104337.
[24]Wang, W., Chen, G., Han, Z. *et al.* 3D numerical simulation of debris-flow motion using SPH method incorporating non-Newtonian fluid behavior. *Nat. Hazards* (2016) **81**: 1981-1998.
[25]Jop, P., Forterre, Y. and Pouliquen, O. A constitutive law for dense granular flows. *Nature* (2006) **441**: 727-730.
[26]Fourtakas, G., Rogers, B.D. and Laurence, D.R. Modelling sediment resuspension in industrial tanks using SPH. *La Houille Blanche* (2013): 39-45.
[27]Iverson, R.M. and Denlinger, R.P. Flow of variably fluidized granular masses across three‐dimensional terrain: 1. Coulomb mixture theory. *J. Geophys. Res-Sol. Ea* (2001) **106**: 537-552.
[28]Han, Z., Su, B., Li, Y. *et al.* Modeling the progressive entrainment of bed sediment by viscous debris flows using the three-dimensional SC-HBP-SPH method. *Water Res* (2020) **182**: 116031.
[29]Han, Z., Su, B., Li, Y. *et al.* Numerical simulation of debris-flow behavior based on the SPH method incorporating the Herschel-Bulkley-Papanastasiou rheology model. *Eng. Geol* (2019) **255**: 26-36.
[30]English, A., Domínguez, J., Vacondio, R. *et al.* Modified dynamic boundary conditions (mDBC) for general-purpose smoothed particle hydrodynamics (SPH): Application to tank sloshing, dam break and fish pass problems. *Comput. Part. Mech* (2022) **9**: 1-15.
[31]Crespo, A., Gómez-Gesteira, M. and Dalrymple, R.A. Boundary conditions generated by dynamic particles in SPH methods. *Cmc-Tech Science Press* (2007) **5**: 173.
[32]Papanastasiou, T.C. Flows of materials with yield. *J. Rheol* (1987) **31**: 385-404.
[33]Manenti, S., Sibilla, S., Gallati, M. *et al.* SPH simulation of sediment flushing induced by a rapid water flow. *J. Hydraul. Eng* (2012) **138**: 272-284.